5. M. DeKeviet, D. Dubbers, C. Schmidt, D. Scholz, U. Spinola, *Phys. Rev. Lett.* **75**, 1919 (1995).
6. A. P. Jardine, J. Ellis, W. Allison, *J. Phys. Condens. Matter* **14**, 6173 (2002).
7. F. Mezei, *Z. Phys.* **255**, 146 (1972).
8. M. Dekeviet, D. Dubbers, M. Klein, M. Schmidt, M. Skrzipczyk, *Surf. Sci.* **337**, 1112 (1997).
9. D. R. Miller, in *Atomic and Molecular Beam Methods*, G. Scoles, Ed. (Oxford Univ. Press, Oxford, 1998).
10. A. P. Jardine, P. Fouquet, J. Ellis, W. Allison, *Rev. Sci. Instrum.* **72**, 3834 (2001).
11. S. Dworski *et al.*, *Rev. Sci. Instrumen.* **75**, 1963 (2004).
12. E. Estermann, O. Stern, *Z. Phys.* **61**, 95 (1930).
13. J. E. Lennard-Jones, A. F. Devonshire, *Nature* **137**, 1069 (1936).
14. R. Frisch, O. Stern, *Z. Phys.* **84**, 430 (1933).
15. H. Hoinkes, H. Wilsch, *in Helium Atom Scattering from Surfaces*, E. Hulpke, Ed. (Springer-Verlag, Berlin, 1992).
16. D. E. Houston, D. E. Frankl, *Phys. Rev. Lett.* **31**, 298 (1973).
17. G. Derry, D. Wesner, S. V. Krishnaswamy, D. R. Frankl, *Surf. Sci.* **74**, 245 (1978).
18. D. R. Frankl, D. Wesner, S. V. Krishnaswamy, G. Derry, T. O'Gorman, *Phys. Rev. Lett.* **41**, 60 (1978).
19. D. A. Wesner, D. R. Frankl, *Phys. Rev. B* **24**, 1798 (1981).
20. G. Brusdeylins, R. B. Doak, J. P. Toennies, *Phys. Rev. B* **27**, 3662 (1983).
21. G. Wolken, *J. Chem. Phys.* **58**, 3047 (1973).
22. W. E. Carlos, G. Derry, D. R. Frankl, *Phys. Rev. B* **19**, 3258 (1979).
23. V. Celli, D. Eichenauer, A. Kaufhold, J. P. Toennies, *J. Chem. Phys.* **83**, 2504 (1985).
24. J. S. Hutchinson, *Phys. Rev. B* **22**, 5671 (1980).
25. G. Armand, J. Lapujoulade, J. R. Manson, *Phys. Rev. B* **39**, 10514 (1989).
26. A. P. Jardine, J. Ellis, W. Allison, *J. Chem. Phys.* **120**, 8724 (2004).
27. A. P. Graham *et al.*, *J. Chem. Phys.* **108**, 7825 (1996).
28. Q. Ge, D. A. King, *J. Chem. Phys.* **111**, 9461 (1999).
29. Q. Ge, D. A. King, *J. Chem. Phys.* **114**, 1053 (2001).
30. P. Fouquet, R. A. Olsen, E. J. Baerends, *J. Chem. Phys.* **119**, 509 (2003).
31. Instrumental development was supported by a Paul Instrument Fund grant. A.P.J. and S.D. are grateful to the University of Cambridge Oppenheimer Trust for support. P.F. is grateful to the European Commission, the Humboldt Foundation, and the Isaac Newton Trust for support. G.A. is grateful to the Gates Cambridge Trust, Gonville & Caius College, and an Overseas Research Studentship (ORS) for support. D.J.R. was supported by an Engineering and Physical Sciences Research Council studentship. G.Y.H.L. was supported by the Cambridge Commonwealth Trust, an ORS, and a Foreign and Commonwealth Office studentship.

30 March 2004; accepted 13 May 2004

Hsp104 Catalyzes Formation and Elimination of Self-Replicating Sup35 Prion Conformers

James Shorter and Susan Lindquist*

The protein-remodeling factor Hsp104 governs inheritance of [*PSI*$^+$], a yeast prion formed by self-perpetuating amyloid conformers of the translation termination factor Sup35. Perplexingly, either excess or insufficient Hsp104 eliminates [*PSI*$^+$]. In vitro, at low concentrations, Hsp104 catalyzed the formation of oligomeric intermediates that proved critical for the nucleation of Sup35 fibrillization de novo and displayed a conformation common among amyloidogenic polypeptides. At higher Hsp104 concentrations, amyloidogenic oligomerization and contingent fibrillization were abolished. Hsp104 also disassembled mature fibers in a manner that initially exposed new surfaces for conformational replication but eventually exterminated prion conformers. These Hsp104 activities differed in their reaction mechanism and can explain [*PSI*$^+$] inheritance patterns.

The yeast prion state [*PSI*$^+$] results from self-perpetuating, dysfunctional, prion aggregates of Sup35 (a translation termination factor) that cause stable, heritable reductions in the fidelity of translation termination (*1*, *2*). The N-terminal, glutamine- and asparagine-rich (N) and highly charged middle (M) domains of Sup35 are necessary and sufficient for Sup35 to transition between the soluble, functional state of Sup35 in [*psi*$^-$] cells and the prion state of [*PSI*$^+$] cells (*1–5*). In [*PSI*$^+$] cells, NM (the N and M domains of Sup35) adopts an amyloid-like conformation (NM) (*1–8*). In vitro, NM spontaneously forms self-propagating, β-sheet–rich amyloid fibers after a characteristic lag phase (*8–12*). Fibers grow rapidly at their ends (*9*, *10*) and truly embody prion conformers, because transforming [*psi*$^-$] cells with in vitro–generated NM fibers, but not with soluble NM, efficiently induces [*PSI*$^+$] (*13*).

[*PSI*$^+$] inheritance depends absolutely on the cellular concentration of Hsp104. Either deletion or overexpression of Hsp104 eliminates [*PSI*$^+$] (*1–6*, *14*, *15*). Hsp104 is a protein-remodeling factor belonging to the AAA+ (Adenosine triphosphatases Associated with diverse Activities) family. Two models might explain the baffling dosage relationship (*1–4*, *6*, *14*, *15*): (i) Hsp104 acts on soluble Sup35 to generate prion conformers through a critical oligomeric intermediate. Excess or insufficient Hsp104 would create imbalances between Hsp104 and Sup35 and perturb amyloidogenic oligomerization. (ii) The disaggregation activity of Hsp104 (*16*) operates on Sup35 fibers to cleave them. Excess Hsp104 would completely annihilate fibers, whereas too little would yield overly large aggregates that are poorly disseminated to progeny and have too few polymerization surfaces to sustain prion propagation. Here we define the direct effects of Hsp104 concentration on the different conformational states of NM, the prion domain of Sup35.

When Hsp104 [together with adenosine triphosphate (ATP) and an ATP regeneration system] was added to unpolymerized NM at substoichiometric concentrations, it greatly accelerated NM polymerization into amyloid fibers (Fig. 1A). Throughout this study, we confirmed the nature of the amyloid fibers by several different techniques (fig. S1) (*17*). Hsp104 completely eliminated the lag phase (reducing T_0, the time before detection of amyloid, from 45 min to undetectable) and accelerated the assembly phase (reducing T_C, the time between the first appearance of amyloid and completion of conversion, from 195 min to 45 min). Titration of several other proteins into NM fibrillization reactions did not stimulate assembly (supporting online text). Electron microscopy (EM) revealed that Hsp104-generated fibers were indistinguishable from spontaneously formed fibers, except that they were slightly shorter (1.1 ± 0.8 μm without Hsp104 versus 0.8 ± 0.4 μm with Hsp104).

If Hsp104-generated NM fibers are relevant to prion propagation, they should seed the fibrillization of unpolymerized NM. We first depleted these fibers of Hsp104, because the remodeling factor would interfere with analysis of seeding efficacy. Consistent with the transient nature of Hsp104-Sup35 interactions (*1*, *18*), Hsp104 was readily removed without codepleting NM (fig. S2). Hsp104-generated NM fibers seeded polymerization just as well as fibers that had been assembled in spontaneous reactions (Fig. 1B) (*17*), which can convert cells from [*psi*$^-$] to [*PSI*$^+$] (*13*). Thus, Hsp104 catalyzes the acquisition of a self-replicating prion conformation.

Amyloid fibers are connected with several devastating neurodegenerative disorders, including Alzheimer's, Parkinson's, and Huntington's diseases (*19–21*). A common feature of amyloidogenesis is the appearance of oligomeric species before fibrillization that may or may not be "on pathway" for fiber assembly (*10–12*, *19*, *20*). An antibody raised against an amyloidogenic peptide associated with Alzheimer's disease, Aβ40, which had been tethered at one end to prevent fibrillization, recognizes β-sheet–rich, oligomeric intermediates of Aβ40 (*20*). It also recognizes oligomeric species of several other amyloidogenic polypeptides including Aβ42, lysozyme, islet amyloid polypeptide,

Whitehead Institute for Biomedical Research, Nine Cambridge Center, Cambridge, MA 02142, USA.

*To whom correspondence should be addressed. E-mail: lindquist_admin@wi.mit.edu

α-synuclein, polyglutamine, insulin, and prion protein (*20*). It does not, however, recognize monomers or mature fibers of these proteins (*20*). We used this antibody to determine the role of oligomers and of Hsp104 in prion assembly.

Unlike an NM-specific antibody, the oligomer-specific antibody recognized neither NM solubilized in urea nor NM fibers (Fig. 1C). However, in spontaneous assembly reactions, it recognized a species that peaked late in the lag phase and was rapidly consumed during the assembly phase (Fig. 1C). This corresponded to an oligomeric form of NM, because the immunoreactive species did not pass through a 100-kD filter [NM is a 28.5-kD protein (fig. S3A)]. Consistent with previous studies (*10*–*12*), the proportion of NM that was present in an oligomeric state and was retained by the 100-kD filter remained constant (~10% of total NM) throughout the lag phase (fig. S3B). Hence, NM forms molten oligomeric complexes rapidly, and these gradually metamorphose into oligomeric species recognized by the conformation-specific antibody (*1*, *10*–*12*).

The oligomer-specific antibody severely inhibited unseeded NM polymerization, even at concentrations 100-fold lower than the NM concentration (Fig. 1D). Thus, NM oligomers recognized by the oligomer-specific antibody are crucial for nucleating polymerization at the end of the lag phase. Conversely, the antibody had no effect on NM polymerization seeded by sonicated NM fibers, even at a 100-fold molar excess over added seed (fig. S4). Therefore, the amyloidogenic oligomer recognized by this antibody is not required for polymerization once fibers have formed. That is, fibers can recruit NM that is not in this amyloidogenic oligomeric form (either monomers or immature oligomers).

Addition of Hsp104 plus ATP to soluble NM caused the immediate appearance of mature oligomers that reacted with the oligomer-specific antibody. This species was rapidly consumed upon fibrillization (Fig. 1C). Thus, Hsp104 eliminates the lag phase in NM polymerization by catalyzing the nascence of the critical amyloidogenic NM oligomer that elicits fibrillization.

We also employed an amyloid-specific antibody, raised against Aβ40 fibers, which also recognizes fibers formed by several other amyloid proteins (*21*). We found that it recognized NM fibers but not unassembled protein (Fig. 1D and fig. S4). In contrast with the oligomer-specific antibody, it inhibited both unseeded and seeded NM fibrillization (Fig. 1D and fig. S4), reinforcing the importance of amyloid conformers in the conversion of NM to the prion state (*13*).

Nonhydrolyzable ATP analogs adenosine 5′-(β-γ-imido) triphosphate (AMP-PNP) and methylene-adenosine 5′-triphosphate (AMP-PCP) supported Hsp104-catalyzed oligomer maturation and fibrillization (Fig. 1E) (*17*), even with hexokinase and glucose present to eliminate trace contaminating ATP (*22*). Adenosine diphosphate (ADP) did not support these activities. These findings were extended with several Hsp104 AAA+ point mutants defective in ATP binding and/or hydrolysis at nucleotide binding domain (NBD)

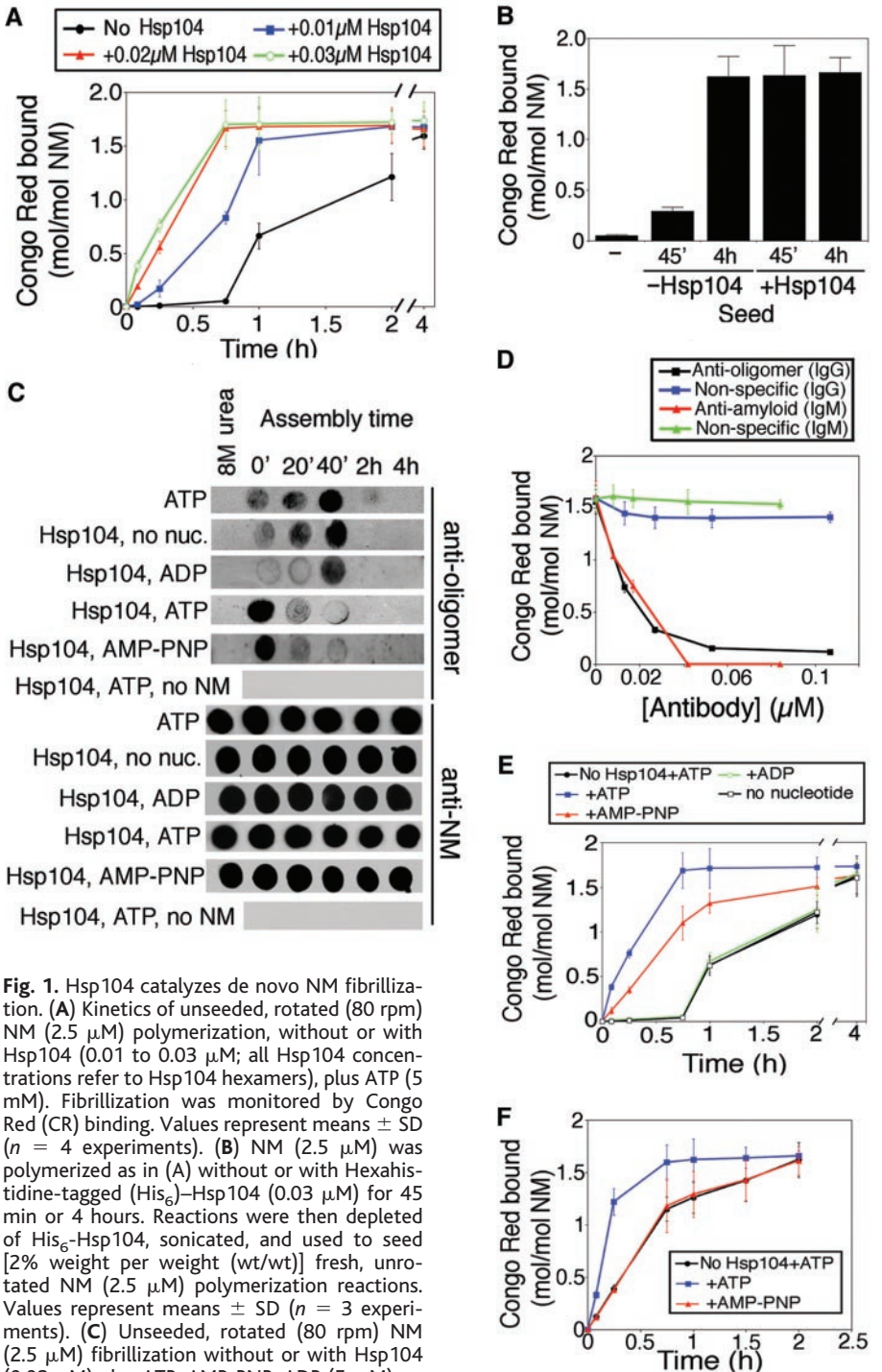

Fig. 1. Hsp104 catalyzes de novo NM fibrillization. (**A**) Kinetics of unseeded, rotated (80 rpm) NM (2.5 μM) polymerization, without or with Hsp104 (0.01 to 0.03 μM; all Hsp104 concentrations refer to Hsp104 hexamers), plus ATP (5 mM). Fibrillization was monitored by Congo Red (CR) binding. Values represent means ± SD (n = 4 experiments). (**B**) NM (2.5 μM) was polymerized as in (A) without or with Hexahistidine-tagged (His_6)–Hsp104 (0.03 μM) for 45 min or 4 hours. Reactions were then depleted of His_6-Hsp104, sonicated, and used to seed [2% weight per weight (wt/wt)] fresh, unrotated NM (2.5 μM) polymerization reactions. Values represent means ± SD (n = 3 experiments). (**C**) Unseeded, rotated (80 rpm) NM (2.5 μM) fibrillization without or with Hsp104 (0.03 μM) plus ATP, AMP-PNP, ADP (5 mM), or no nucleotide. At various times, reactions were applied to nitrocellulose and probed with oligomer-specific antibody or NM-specific antibody. The far left lane contains NM in 8 M urea. (**D**) Unseeded, rotated (80 rpm) NM (2.5 μM) fibrillization after 6 hours with increasing concentrations of either anti-oligomer immunoglobulin G (IgG), nonspecific IgG, anti-amyloid IgM, or nonspecific IgM. Values represent means ± SD (n = 4 experiments). (**E**) Reactions were performed as in (A) without or with Hsp104 (0.03 μM) plus either ATP (5 mM), AMP-PNP (5 mM), ADP (5 mM), or no nucleotide. Values represent means ± SD (n = 3 experiments). (**F**) Seeded (2% wt/wt), unrotated NM (2.5 μM) fibrillization without or with Hsp104 (0.03 μM) plus ATP or AMP-PNP (5 mM). Values represent means ± SD (n = 3 experiments).

1 or 2, which have previously been shown to affect [*PSI*$^+$] inheritance in vivo (*4*, *15*, *23*, *24*) (supporting online text and fig. S5). Hsp104 mutants that interfered with hexamerization, or with the ability to bind ATP at either NBD, failed to induce NM fibrillization (fig. S5). Mutants that could bind but not hydrolyze ATP accelerated polymerization, but not as well as wild-type protein (fig. S5). Thus, ATP hydrolysis is not required per se, but hydrolysis at both NBDs maximizes the rate of Hsp104-catalyzed NM fibrillization.

To investigate the unusual dosage relationship between Hsp104 and prion replication, we tested higher Hsp104 concentrations. When the stoichiometry of NM monomers to Hsp104 hexamers was altered from 250:1 to 15:1, NM polymerization was abolished (Fig. 2A and fig. S6) (*17*). Hsp104 blocked fibrillization by coupling ATP hydrolysis to the elimination of amyloidogenic NM oligomers (Fig. 2B). At high concentrations, Hsp104 also eliminated fibrillization with AMP-PNP, ADP, and even without nucleotide. However, successively higher Hsp104 concentrations were required in each case (fig. S6A) (*17*). Without ATP, Hsp104 did not eliminate oligomers but simply prevented their maturation (Fig. 2B) (*22*). Corroboratively, Hsp104 point mutants with reduced hexamerization or ATPase activity inhibited NM fibrillization, but with decreased efficiency (supporting online text and fig. S6B). Thus, Hsp104 can passively inhibit NM fibrillization, perhaps through transiently binding NM. Because AMP-PNP allows a more severe inhibition at lower Hsp104 levels [median inhibitory concentration (IC_{50}) ~ 0.2 μM] than ADP (IC_{50} ~ 3.1 μM) or in the absence of nucleotide (IC_{50} ~ 7.6 μM), Hsp104 may preferentially engage NM in an ATP-bound conformation. However, inhibition is potentiated when coupled to ATP hydrolysis (IC_{50} ~ 0.1 μM) and contingent oligomer remodeling.

Next, we asked if the ability of Hsp104 to accelerate NM fibrillization during the assembly phase is due to the same activity that eliminates the lag phase (that is, the production of amyloidogenic oligomers) or represents a distinct activity. We found that Hsp104 promoted polymerization in reactions that did not require the production of new oligomers, because they were seeded with preformed fibers. However, this activity required ATP hydrolysis. Hsp104 plus AMP-PNP, which was able to catalyze de novo assembly of oligomeric intermediates, did not accelerate seeded assembly (Fig. 1F) (*17*). Moreover, promoting assembly was independent of amyloidogenic oligomers, because blocking their maturation with oligomer-specific antibody had no effect on seeded assembly (fig. S4). Thus, Hsp104 also promotes fiber assembly by a reaction mechanism distinct from nucleation.

We postulated that accelerating the assembly phase might involve an effect of Hsp104 on NM fibers. Indeed, when Hsp104 (with ATP and an ATP regeneration system) was added to NM fibers, it disassembled them (Fig. 3, A to C, and fig. S7). The reaction exhibited a steep Hsp104 concentration dependence, implying a cooperative reaction mechanism (Fig. 3, A and B, and fig. S7). Hsp104 briskly diminished the mean fiber length from ~1.1 ± 0.8 μm to ~0.2 ± 0.1 μm after 5 min, and to ~0.1 ± 0.05 μm after 10 min (Fig. 3C). This was superficially reminiscent of sonication, which generates short fibers and creates additional polymerization surfaces (*10*). Indeed, the short fibers produced by brief Hsp104 treatments markedly increased seeding activity (Fig. 3D) (*17*).

With longer incubations, fibers were completely obliterated (Fig. 3, B and C, and fig. S7). The final disassembly products were devoid of seeding activity (Fig. 3D) (*17*), distinguishing them from short fibers. In the early phases of disassembly, Hsp104 released amyloidogenic NM oligomers from fibers (Fig. 3E). Later, these oligomers were no longer apparent (Fig. 3E), which correlates with the annulment of seeding activity. Thus, when Hsp104 disassembles NM fibers, it initially creates additional polymerization surfaces as well as new amyloidogenic oligomers. However, Hsp104 eventually destroys seed, emancipating NM from the self-replicating prion conformation.

Unlike the formation of amyloidogenic oligomers, fiber shortening and the eradication of seeding activity by Hsp104 required ATPase activity. It was not supported by AMP-PNP, AMP-PCP, ADP, or the absence of nucleotide (Fig. 3F). Furthermore, hydrolysis was required at both NBD1 and NBD2. Hsp104 mutants defective in ATP hydrolysis at either NBD could not depolymerize fibers (fig. S8).

The ability of Hsp104 to promote the assembly and disassembly of NM fibers was highly specific. Hsp70 and Hsp40 chaperones can also affect [*PSI*$^+$] in vivo (*1*, *2*). They also exerted effects on NM fibrillization (*25*), but they were not required for either assembly or disassembly of NM fibers by Hsp104. Moreover, they could not, on their own or in combination, promote NM fiber assembly or disassembly (*25*). A prokaryotic homolog of Hsp104, ClpB, and another eukaryotic AAA+ protein, Cdc48p, were also ineffective in promoting NM fiber assembly or disassembly (*22*).

Our results establish the mechanisms by which Hsp104 may control the formation, replication, and curing of [*PSI*$^+$]. By uncovering multiple Hsp104 remodeling activities on NM, the prion domain of Sup35, we have recreated the unusual dosage relationship between [*PSI*$^+$] and Hsp104 in vitro and reconciled previous models concerning the role of Hsp104 in prion inheritance (*1*–*4*, *6*, *14*, *15*). Two activities promote prion formation and replication: (i) At low concentrations, Hsp104 acts on soluble NM and catalyzes assembly of critical oligomeric intermediates that nucleate fibrillization; and (ii) Hsp104 fragments amyloid fibers to create new ends for polymerization and facilitate partitioning of seeds to progeny. Three activities promote prion curing: (i) At high concentrations, Hsp104 passively inhibits oligomer maturation; (ii) Hsp104 couples ATP hydrolysis to the elimination of amyloidogenic oligomers; and (iii) Hsp104 couples ATPase activity to the disassembly of fibers into non-amyloidogenic species. These activities employ different modes of Hsp104 action. We previously showed that Hsp104 binds polylysine in a highly cooperative manner, triggering a cascade of events that couple ATP hydrolysis at NBD2 to conformational change in the coiled-coil middle domain and to hydrolysis at NBD1 (*26*). The M region of Sup35, which resides on the exterior of NM fibers (*10*), is lysine-rich (*8*). Cooperative interactions between M and Hsp104, coupled to additional interactions with the glutamine-rich N domain (*27*), may serve as a fulcrum for force application by Hsp104 to separate the intermolecular β-sheet interfaces of N that maintain fiber integrity (*10*, *26*, *28*). Consistent with this, changes in the M region alter the relationship between Hsp104 and

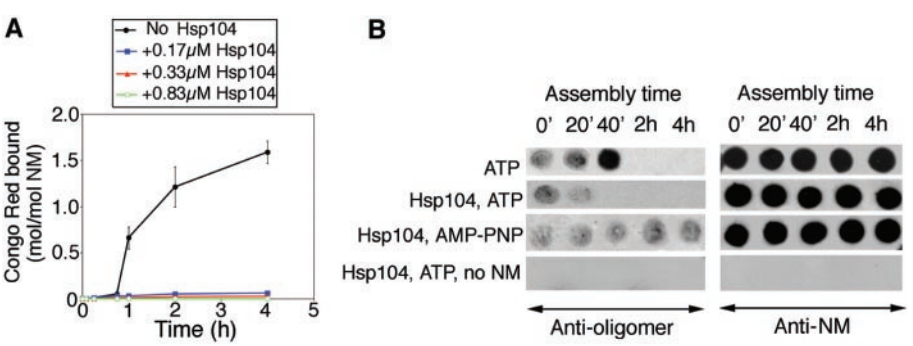

Fig. 2. Hsp104 abolishes NM fibrillization. (**A**) Kinetics of unseeded, rotated (80 rpm) NM (2.5 μM) polymerization without or with Hsp104 (0.17 to 0.83 μM) plus ATP (5 mM). Fibrillization was quantified by CR binding. Values represent means ± SD (n = 4 experiments). (**B**) Unseeded, rotated (80 rpm) NM (2.5 μM) fibrillization without or with Hsp104 (0.3 μM) plus ATP or AMP-PNP (5 mM). At various times, reactions were applied to nitrocellulose and probed with oligomer-specific antibody or NM-specific antibody.

[*PSI*$^+$] inheritance (*5*). Hsp104 promotes assembly of amyloidogenic oligomers that nucleate fibrillization, requiring ATP binding at both NBDs but not hydrolysis. Hsp104 may provide a catalytic surface on which NM molecules transiently converge to attain the amyloidogenic oligomeric conformation. Alterations in the Sup35:Hsp104 concentration ratio or Hsp104 activity (e.g., by heat shock) can radically shift the balance between these activities and either promote or eliminate self-replicating prion conformers and the [*PSI*$^+$] phenotype (*1*, *4*, *14*, *15*, *23*, *24*). The effects of Hsp104 on NM fibrillization and disassembly could be reconstituted with full length Sup35, reinforcing their physiological significance (*25*).

We also establish that an amyloidogenic oligomer is an obligate intermediate for nucleating prion formation de novo. Previously, we postulated (*10*–*12*) that intrinsically unfolded NM monomers may have too many accessible conformations to find a stable fold and that molten oligomers might allow NM to sample intermolecular interactions that stabilize β-strands to form amyloidogenic nuclei (*10*–*12*). It may be that many amyloids assemble by a related mechanism (*10*, *19*, *20*). An antibody that recognizes a common conformational feature of oligomers observed for many disease-associated amyloids also recognizes the amyloidogenic intermediate of NM. Oligomers may also be the most toxic species in the protein misfolding diseases (*19*, *20*). Rapid conversion of oligomers to amyloid fibers driven by Hsp104 may explain why the conformational conversion of Sup35 to a prion state is not toxic in yeast, because the oligomeric species would be short-lived. It seems likely that Hsp104 coevolved with Sup35 to regulate [*PSI*$^+$], functioning as the minimal machinery controlling prion conformation and inheritance. [*PSI*$^+$] profoundly changes the spectrum of conditions in which yeast cells thrive, and Hsp104 may therefore provide one link between heritable changes in phenotype and environmental contingency (*1*, *2*). Our studies reinforce that amyloids are not necessarily intractable, pathogenic entities but can be harnessed and tightly regulated for advantageous purposes (*1*, *2*, *19*, *29*). An accurate understanding of this regulation will enlighten analogous complexities in amyloidogenic events that underpin protein misfolding diseases (*19*), protein-based genetics (*1*, *2*), and molecular memories (*29*).

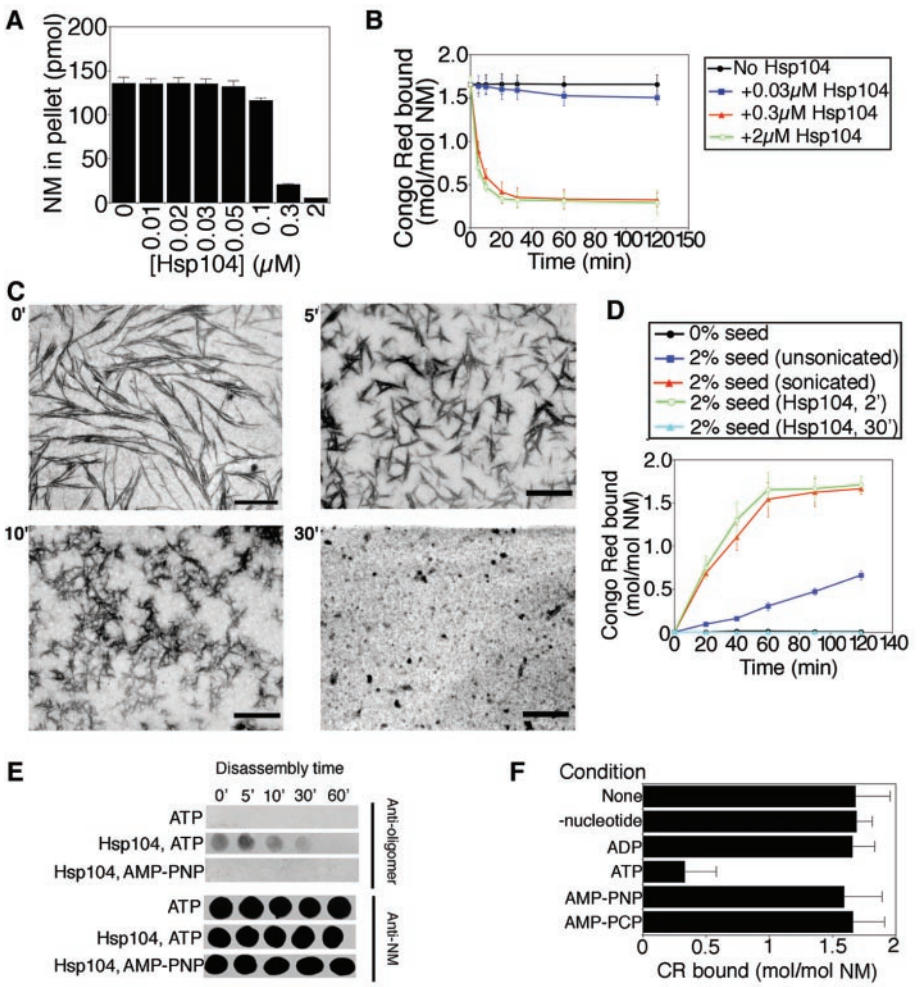

Fig. 3. Hsp104 couples ATP hydrolysis to NM fiber and oligomer disassembly. (**A**) NM (2.5 μM) was incubated for 6 hours with rotation (80 rpm) to generate fibers and then incubated with Hsp104 (0 to 2 μM) for 20 min at 25°C. Disassembly was assessed by sedimentation. Values represent means ± SD (n = 3 experiments). (**B**) Kinetics of Hsp104 (0 to 2 μM) induced NM fiber disassembly monitored by CR binding. Values represent means ± SD (n = 3 experiments). (**C**) NM fibers (2.5 μM monomer) were incubated with Hsp104 (2 μM) for 0 to 30 min, and reactions were processed for EM at various times. Scale bars, 0.25 μm. (**D**) NM fibers (2.5 μM monomer) were either left untreated, sonicated, or treated with His_6-Hsp104 (0.3 μM) for 2 min or 30 min. Reactions were then depleted of Hsp104 and used to seed (2% wt/wt) fresh, unrotated NM (2.5 μM) polymerization. Values represent means ± SD (n = 3 experiments). (**E**) NM fibers (2.5 μM monomer) were incubated without or with Hsp104 (2 μM) plus ATP (5 mM) or AMP-PNP (5 mM) for 0 to 60 min. At various times, reactions were applied to nitrocellulose and probed with oligomer-specific antibody or NM-specific antibody. (**F**) NM fibers (2.5 μM monomer) were incubated (for 30 min at 25°C) with Hsp104 (2 μM) and no nucleotide, ADP (5 mM), ATP (5 mM), AMP-PNP (5 mM), or AMP-PCP (5 mM). Values represent means ± SD (n = 3 experiments).

References and Notes

1. T. R. Serio, S. L. Lindquist, *Adv. Protein Chem.* **59**, 391 (2001).
2. S. M. Uptain, S. Lindquist, *Annu. Rev. Microbiol.* **56**, 703 (2002).
3. S. V. Paushkin, V. V. Kushnirov, V. N. Smirnov, M. D. Ter-Avanesyan, *EMBO J.* **15**, 3127 (1996).
4. M. M. Patino, J. J. Liu, J. R. Glover, S. Lindquist, *Science* **273**, 622 (1996).
5. J. J. Liu, N. Sondheimer, S. L. Lindquist, *Proc. Natl. Acad. Sci. U.S.A.* **99** (suppl. 4), 16446 (2002).
6. D. S. Kryndushkin, I. M. Alexandrov, M. D. Ter-Avanesyan, V. V. Kushnirov, *J. Biol. Chem.* **278**, 49636 (2003).
7. Y. Kimura, S. Koitabashi, T. Fujita, *Cell Struct. Funct.* **28**, 187 (2003).
8. J. R. Glover *et al.*, *Cell* **89**, 811 (1997).
9. A. H. DePace, J. S. Weissman, *Nature Struct. Biol.* **9**, 389 (2002).
10. T. R. Serio *et al.*, *Science* **289**, 1317 (2000).
11. T. Scheibel, S. L. Lindquist, *Nature Struct. Biol.* **8**, 958 (2001).
12. T. Scheibel, J. Bloom, S. L. Lindquist, *Proc. Natl. Acad. Sci. U.S.A.* **101**, 2287 (2004).
13. M. Tanaka, P. Chien, N. Naber, R. Cooke, J. S. Weissman, *Nature* **428**, 323 (2004).
14. Y. O. Chernoff, S. L. Lindquist, B. Ono, S. G. Inge-Vechtomov, S. W. Liebman, *Science* **268**, 880 (1995).
15. R. D. Wegrzyn, K. Bapat, G. P. Newnam, A. D. Zink, Y. O. Chernoff, *Mol. Cell. Biol.* **21**, 4656 (2001).
16. J. R. Glover, S. Lindquist, *Cell* **94**, 73 (1998).
17. Very similar results were obtained when fibrillization was monitored by sodium dodecyl sulfate–resistance, sedimentation, EM, thioflavin T (ThT) fluorescence, 8-anilino-naphthalene-sulfonic acid (ANS) fluorescence, protease resistance, and turbidity.
18. E. C. Schirmer, S. Lindquist, *Proc. Natl. Acad. Sci. U.S.A.* **94**, 13932 (1997).
19. M. E. Huff, W. E. Balch, J. W. Kelly, *Curr. Opin. Struct. Biol.* **13**, 674 (2003).
20. R. Kayed *et al.*, *Science* **300**, 486 (2003).
21. B. O'Nuallain, R. Wetzel, *Proc. Natl. Acad. Sci. U.S.A.* **99**, 1485 (2002).
22. J. Shorter, S. Lindquist, unpublished data.
23. D. A. Hattendorf, S. L. Lindquist, *Proc. Natl. Acad. Sci. U.S.A.* **99**, 2732 (2002).
24. D. A. Hattendorf, S. L. Lindquist, *EMBO J.* **21**, 12 (2002).
25. J. Shorter, S. Lindquist, in preparation.
26. A. G. Cashikar *et al.*, *Mol. Cell* **9**, 751 (2002).
27. S. Narayanan, B. Bosl, S. Walter, B. Reif, *Proc. Natl. Acad. Sci. U.S.A.* **100**, 9286 (2003).
28. S. Lee *et al.*, *Cell* **115**, 229 (2003).

29. K. Si, S. Lindquist, E. R. Kandel, *Cell* **115**, 879 (2003).
30. We are indebted to A. Cashikar for expert advice and assistance, Lindquist lab members for comments on the manuscript, C. Glabe for oligomer-specific antibody, R. Wetzel for antibody to amyloid, N. Watson for EM assistance, and F. Tsai for purified ClpB from *Thermus thermophilus*. Supported by a Charles A. King Trust postdoctoral fellowship (J.S.) and NIH grant no. GM25874 and a DuPont MIT Alliance grant (S.L.).

Supporting Online Material
www.sciencemag.org/cgi/content/full/1098007/DC1
Materials and Methods
SOM Text
Figs. S1 to S8
References and Notes

17 March 2004; accepted 13 May 2004
Published online 20 May 2004;
10.1126/science.1098007
Include this information when citing this paper.

Dynamics of Single mRNPs in Nuclei of Living Cells

Yaron Shav-Tal,[1] Xavier Darzacq,[1] Shailesh M. Shenoy,[1] Dahlene Fusco,[1] Susan M. Janicki,[2] David L. Spector,[2] Robert H. Singer[1*]

Understanding gene expression requires the ability to follow the fate of individual molecules. Here we use a cellular system for monitoring messenger RNA (mRNA) expression to characterize the movement in real time of single mRNA-protein complexes (mRNPs) in the nucleus of living mammalian cells. This mobility was not directed but was governed by simple diffusion. Some mRNPs were partially corralled throughout the nonhomogenous nuclear environment, but no accumulation at subnuclear domains was observed. Following energy deprivation, energy-independent motion of mRNPs was observed in a highly ATP-dependent nuclear environment; movements were constrained to chromatin-poor domains and excluded by newly formed chromatin barriers. This observation resolves a controversy, showing that the energetic requirements of nuclear mRNP trafficking are consistent with a diffusional model.

Recent technological developments have facilitated imaging of single RNA molecules in the cytoplasm of living cells (*1*). We have developed a cellular system in which the expression of a transgene array can be followed sequentially in single living cells, and we have previously analyzed the particular chromatin-related modifications occurring at this specific locus from a silenced state throughout its transcriptional activation (*2*). Here we use this system to address the mechanism by which individual mRNA transcripts move within the nucleoplasm after release from the transcription site.

In this system, a genetic locus, its transcribed mRNAs, and the translated protein were rendered visible in cells after electroporation with the cyan fluorescent protein (CFP) or the red fluorescent protein (RFP)–lac repressor protein (marks the genomic locus), yellow fluorescent protein (YFP)–MS2 (labels the mRNA), and pTet-On (for transcriptional induction) (*3*). Transcriptional activation by doxycycline induced the unfolding of the integrated locus (*4*) and the recruitment of the YFP-MS2 protein to the locus as a result of the specific labeling of the nascent transcripts bearing the MS2 stem loops. Minutes after induction (15 to 30 min), the MS2 signal began accumulating in the nucleoplasm in a particulate pattern suggestive of mRNA-protein complexes (mRNPs). At later times (1 to 2 hours after induction), mRNPs were detected in the cytoplasm in conjunction with the appearance of cyan fluorescent protein (CFP)–labeled peroxisomes, demonstrating that the tagged RNA was both correctly exported and translated (fig. S1, A to D). These components of the gene expression pathway could be detected simultaneously in living cells (*3*) [Movies S1 to S5 (*5*)].

The presence of the nascent RNAs at the site of transcription was verified using fluorescent in situ hybridization (FISH) on fixed cells with two different probes either to the MS2 repeats (located in the middle of the transcript) or to the β globin exon (3′ end). Both probes hybridized at the active locus, indicating that the complete pre-mRNA transcripts were retained at the transcription site before release (fig. S2, A to D). Colocalization of the mRNA signal (FISH) with the YFP signal demonstrated that the particles visualized in living cells were mRNPs (*3*). RNA quantification with single-molecule sensitivity was performed on deconvolved FISH images to a single target sequence in the 3′ end of the transcript (*6*). The majority (~70%) of transcripts hybridized with a single probe, indicating that these nuclear mRNPs represent single RNA transcripts (fig. S2, E to I). Imaging of the mRNPs in fixed or living cells showed that mRNPs were excluded from the nucleolus (*3*) [Movie S5 (*5*)] and that apart from the transcription site, no site of mRNP accumulation could be detected.

Movements of nuclear mRNPs were followed by sequential imaging of living cells, and the obtained signal was enhanced by deconvolution (Fig. 1, A to C). Live cells at early times after induction (up to 30 min) presenting a low concentration of mRNPs were used to continuously track individual particles and study their motion (Fig. 1D). Single-particle tracking (SPT) was performed on mRNPs that remained in focus for a minimum of eight consecutive frames (>3 s) (Fig. 1, E to H) [movies S6 to S10 (*5*)] (*3*). Total distances traveled for tracked mRNPs were from 2 to 10 μm (mean 5 μm), and mean velocities ranged from 0.3 to 0.8 μm/sec (fig. S3A). These mRNPs displayed a diffusive pattern of movement (Fig. 1E) following a simple diffusion model $\langle r^2 \rangle = 4Dt$ (Fig. 1J) (*3*). The diffusion coefficients at 37°C (D_{37}) ranged from 0.01 to 0.09 μm^2/sec (mean 0.04 μm^2/sec) (Fig. 1K). The mean square displacement (MSD) plotted over time Δt was linear in 58% of the cases, characteristic of simple diffusion (Fig. 1J); for 42% of the mobile mRNPs, the plots began linearly but reached a plateau (Fig. 1J), characteristic of corralled diffusion (Fig. 1F). This result indicated the presence of barriers hindering the movement of the mRNPs. Directed movements in the nucleus were not seen among the tracked particles or observed in the overall population of particles imaged (Fig. 1K), although directed translocations were easily detected for cytoplasmic CFP peroxisomes by using our SPT algorithm (*3*) (fig. S3C). Extremely confined movements were observed for transcription sites and for some mRNPs (less than 1% of detectable mRNPs) (Fig. 1I and fig. S3B). These mRNPs were confined within small nucleoplasmic volumes. Observations of living cells (*3*) indicated that once mRNPs were released from the transcription site, their movements through the nucleoplasm on the way to the nuclear pore were rarely hindered by stable interactions with nuclear substructures. Altogether, these data indicated that nucleoplasmic mRNP movement was governed by laws of simple diffusion and was not directional.

Fluorescence recovery after photobleaching (FRAP) of the tagged mRNPs was followed over time, and the mean diffusion coefficient (D_{37}) of these mRNPs was calculated to be 0.09 ± 0.006 μm^2/sec (Fig. 2, A and B), corroborating the SPT data. As with SPT, an immobile fraction was not observed.

We then addressed the movement of mRNPs present in the vicinity of the transcription site, using a third technique. By use of a photoactivatable form of green fluorescent protein (GFP)

[1]Departments of Anatomy and Structural Biology and Cell Biology, Albert Einstein College of Medicine, Bronx, NY 10461, USA. [2]Cold Spring Harbor Laboratory, 1 Bungtown Road, Cold Spring Harbor, NY 11724, USA.

*To whom correspondence should be addressed. E-mail: rhsinger@aecom.yu.edu